Active Noise Control Over Space: A Wave Domain Approach

Jihui Zhang, *Student Member, IEEE,* Thushara D. Abhayapala, *Senior Member, IEEE,* Wen Zhang, *Member, IEEE,* Prasanga N. Samarasinghe, *Member, IEEE,* and Shouda Jiang

***Abstract*—Noise control and cancellation over a spatial region is a fundamental problem in acoustic signal processing. In this paper, we utilize wave-domain adaptive algorithms to iteratively calculate the secondary source driving signals and to cancel the primary noise field over the control region. We propose wave-domain active noise control algorithms based on two minimization problems, (i) minimizing the wave-domain residual signal coefficients and (ii) minimizing the acoustic potential energy over the region, and derive the update equations with respect to two variables, (a) the loudspeaker weights and (b) wave-domain secondary source coefficients. Simulation results demonstrate the effectiveness of the proposed algorithms, more specifically the convergence speed and the noise cancellation performance in terms of the noise reduction level and acoustic potential energy reduction level over the entire spatial region.**

***Index Terms*—Active noise control (ANC), wave domain, multichannel, spatial noise, reverberant room.**

I. Introduction

A. Motivation and Background

Active noise control (ANC), or noise cancellation, employs secondary sound sources to generate secondary signals, which collectively cancel the primary sound field [1], [2]. In applications, such as noise cancellation in aircraft [3] and automobiles [4]–[7], the control zone is large, which requires noise cancellation to be performed over the entire region, instead of at some spatial points. Furthermore, real noise fields are often time-varying and unknown, which requires an adaptive algorithm to iteratively calculate the secondary source driving functions and to produce the secondary sound field.

ANC over space is often approached via multichannel ANC systems with multiple sensors and multiple secondary sources [8]–[10], employing either feed-forward [11] or feedback control systems [12], [13]. Conventional multichannel ANC algorithms in the frequency domain [14]–[16] perform noise cancellation directly on a set of multiple observation points (MP) in the control region, which are fairly straightforward and are widely used in practice [17]. These control systems minimize the sum of the squared pressures, which is equal to minimizing the potential energy density at the microphone locations. Although these approaches lead to significant noise reduction at the target points, the consistency over a continuous spatial region is low.

To overcome this problem and to enlarge the control region, some researchers have proposed ANC systems based on energy density. By utilizing the acoustic energy density sensors [18], Parkins captured more global information in the enclosure and minimized the acoustic energy density (AED) [19]. Similar methods have been proposed such as minimizing the acoustic potential energy (APE) [20], and minimizing the generalized acoustic energy density (GED) [21]. Montazeri described the acoustic potential energy in terms of room modes, which depends greatly on the room geometry [22].

Recently, ANC over space has been approached via Wave Field Synthesis (WFS) based adaptive algorithms [23]–[25] and cylindrical/spherical harmonics expansion based *wave domain* adaptive algorithms [26], [27]. Please note that in this manuscript, we use the terminology "wave-domain signal processing" to refer to harmonics (cylindrical/spherical) based sound field processing. Harmonics based wave-domain signal processing is a technique commonly used for spatial sound field recording/reproduction over spatial regions using discrete transducer arrays. The principle of harmonic representation of sound fields is to use fundamental solutions of the Helmholtz wave-equation as basis functions to express sound over a spatial region. Thus, the sound field can be thought of as superimposed set of orthogonal and continuous basis fields (cylindrical/spherical harmonics) with corresponding knobs to control relative weights (coefficients) of each basis wave field. Since wave-domain signal processing controls propagating sound fields in whole rather than a distributed set of target points, it naturally provides a more insightful and efficient method for ANC over space.

Initial work on harmonics based solutions to ANC appeared in [26], [27]. The authors use cylindrical/spherical harmonics as basis functions and their respective coefficients to represent the noise field and secondary field over the desired spatial region. Instead of minimizing the sum of the squared error signals [28], wave-domain ANC tends to minimize the harmonic coefficients, which in turn control the entire spatial region directly. Authors of [26], [27] showed that wave-domain ANC can achieve significant noise cancellation over the entire region of interest with faster convergence speeds.

J. Zhang is with the Research School of Engineering, College of Engineering and Computer Science, The Australian National University, Canberra, ACT 2601, Australia. She is also with School of Electrical Engineering and Automation, Harbin Institute of Technology, Harbin Heilongjiang 150001, China (e-mail: jihui.zhang@anu.edu.au).

T.D. Abhayapala and P.N. Samarasinghe are with the Research School of Engineering, College of Engineering and Computer Science, The Australian National University, Canberra, ACT 2601, Australia (e-mail: thushara.abhayapala@anu.edu.au; prasanga.samarasinghe@anu.edu.au).

W. Zhang is with Center of Intelligent Acoustics and Immersive Communications, School of Marine Science and Technology, Northwestern Polytechnical University, Shaanxi 710072, China (e-mail: wen.zhang@nwpu.edu.cn).

S. Jiang is with School of Electrical Engineering and Automation, Harbin Institute of Technology, Harbin Heilongjiang 150001, China (e-mail: jsd@hit.edu.cn).

B. Approach and Novel Contributions

In this paper, for the first time, we present a comprehensive analysis on adaptive wave-domain ANC based on a feedback control system, while studying multiple cost functions and multiple update algorithms. We use a a microphone array to measure the residual signals and a loudspeaker array to generate the secondary sound signals. We utilize the harmonic coefficients to characterize the noise field and calculate the acoustic potential energy. In existing spatial ANC work, the adaptive algorithms are based on minimizing residual sound field coefficients and updating the secondary sound field coefficients to update the secondary source weights. In this paper, we develop normalized wave-domain ANC algorithms in two different ways: (i) minimizing the residual sound field coefficients and (ii) minimizing the acoustic potential energy of the residual sound field. We also derive the update equations with respect to two variables: (a) the loudspeaker weights and (b) secondary sound field coefficients. Thus, resulting four different method of implementing harmonics based wave-domain ANC systems. We compare these four methods respect to each other as well as with the the conventional multi-point method. We show that there are trade-offs in selecting each one of the four algorithm over the other. To the best of our knowledge, the detailed analysis of these four wave-domain adaptive algorithms have not been reported in the literature. The proposed algorithms are shown to give better convergence results and improve noise reduction performance within the control region when compared to the conventional multi-point method.

The rest of the paper is organized as follows. In Section II we formulate the spatial noise cancellation problem and the ANC system in the wave domain. The four variants of wave-domain multichannel ANC algorithms are proposed in Section III. We demonstrate the simulation results to compare the ANC performance of the proposed wave-domain methods and the conventional multi-point method in Section IV, and draw some conclusions in Section V.

II. Problem Formulation

A. System Model

In this section, we address the problem of ANC to cancel the noise over a spatial region. Let the interested control zone be a circular region (S) with a radius R_1. We assume that the noise sources are located outside the control region.

We consider an ANC system in two-dimensional space using (i) a single microphone array on the boundary of the control region to measure the residual signals and (ii) a single loudspeaker array outside the region to generate the secondary sound field [26], as shown in Fig.1. The theory we develop in this paper can be extended to 3-D space.

Any arbitrary observation point within the control region is denoted as $\boldsymbol{x} \equiv \{r, \phi_{\boldsymbol{x}}\}$. In the ANC system, the residual signal at this point is given by

$$e(\boldsymbol{x}, k) = v(\boldsymbol{x}, k) + s(\boldsymbol{x}, k), \tag{1}$$

where $k = 2\pi f/c$ is the wave number, f is the frequency, c is the speed of sound propagation, $v(\boldsymbol{x}, k)$ is the noise signal

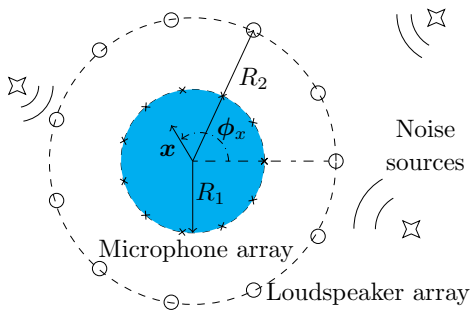

Fig. 1: A spatial ANC region (black) consists of a circular microphone array of radius R_1 and a circular loudspeaker array of radius R_2.

and $\boldsymbol{s}(\boldsymbol{x}, k)$ is the secondary sound field generated by the loudspeakers.

The secondary sound field generated by the loudspeaker array can be represented by

$$s(\boldsymbol{x}, k) = \sum_{q=1}^{Q} d_q(k) G(\boldsymbol{x}|\boldsymbol{y}_q, k), \tag{2}$$

where $d_q(k)$ is the driving signal of the q^{th} loudspeaker, and $G(\boldsymbol{x}|\boldsymbol{y}_q, k)$ denotes the acoustic transfer function (ATF) between the q^{th} loudspeaker and the observation point $\boldsymbol{x}$. For example, for sound propagation in free field, $G(\boldsymbol{x}|\boldsymbol{y}_q, k) = \frac{i}{4}\mathcal{H}_0^{(2)}(k\|\boldsymbol{y}_q - \boldsymbol{x}\|)$, where $\mathcal{H}_0^{(2)}(\cdot)$ is the zero$^{\text{th}}$-order Hankel function of the second kind.

Instead of using the measurements on the microphone points directly, the wave domain approach employs the wave equation solutions as basis functions to express the sound field over the entire spatial region of interest, and designs the secondary signals accordingly. Below we transform each component in (1) and (2) into the wave domain.

B. Primary noise field

The cylindrical harmonic based wave equation solution decomposes any homogeneous incident wave field $v(\boldsymbol{x}, k)$ observed at $\boldsymbol{x}$ into

$$v(\boldsymbol{x}, k) = \sum_{m=-\infty}^{\infty} \beta_m(k) J_m(kr) \exp(im\phi_{\boldsymbol{x}}), \tag{3}$$

where $J_m(\cdot)$ is the Bessel function of order m and $\exp(\cdot)$ denotes the exponential function [29]. The decomposition coefficients $\beta_m(k)$ represent the primary noise field in the wave domain. Within the circular region $r \leq R_1$, we can use a finite number of modes to approximate[1] the noise field [30], thus (3) reduces to

$$v(\boldsymbol{x}, k) \approx \sum_{m=-M}^{M} \beta_m(k) J_m(kr) \exp(im\phi_{\boldsymbol{x}}), \tag{4}$$

where $M = \lceil ekr/2 \rceil$ [30], [31].

[1]The infinite summation in (3) can be truncated at $M = \lceil ekr/2 \rceil$ [30], [31] due to inherent properties of Bessel functions

C. Secondary sound field

Using the cylindrical harmonic expansion, the generated secondary sound field inside the control region can also be represented by

$$s(\boldsymbol{x},k) \approx \sum_{m=-M}^{M} \gamma_m(k) J_m(kr) \exp(im\phi_{\boldsymbol{x}}), \tag{5}$$

where coefficients $\gamma_m(k)$ represent the secondary sound field in the wave domain.

The ATF in (2) can be parameterized [32] as

$$G(\boldsymbol{x}|\boldsymbol{y}_q,k) \approx \sum_{m=-M}^{M} T_{m,q}(k) J_m(kr) \exp(im\phi_{\boldsymbol{x}}), \tag{6}$$

where $T_{m,q}(k)$ are the ATF coefficients in the wave domain and assumed to be prior knowledge obtained from pre-calibration.

By substituting (5) and (6) into (2), we can get

$$\gamma_m(k) = \sum_{q=1}^{Q} d_q(k) T_{m,q}(k), \text{ for } m = -M, \cdots, M. \tag{7}$$

Therefore, in matrix form, the relationship between the secondary source decomposition coefficients and the loudspeaker weights are given by

$$\boldsymbol{\gamma}(k) = \boldsymbol{T}\boldsymbol{d}(k), \tag{8}$$

where $\boldsymbol{T}$ is a $(2M+1) \times Q$ matrix with the (i,j) element given by $T_{i-M-1,j}$, $\boldsymbol{\gamma}$ is the secondary coefficients vector with the (i) element given by $\gamma_{i-M-1}(k)$, and $\boldsymbol{d}$ is the vector of loudspeaker driving signals.

D. Residual signals

Substituting (4) and (5) into (1), the residual signals can be represented by

$$e(\boldsymbol{x},k) \approx \sum_{m=-M}^{M} \underbrace{(\beta_m(k) + \gamma_m(k))}_{\alpha_m(k)} J_m(kr) \exp(im\phi_{\boldsymbol{x}}), \tag{9}$$

where $\alpha_m(k)$ is the residual signal decomposition coefficients. In our ANC system, $e(\boldsymbol{x},k)$ are the frequency domain sound pressure measured by the error microphones. From (9), we can obtain the wave domain $\alpha_m(k)$, which is a good indicator of the residual sound field over the entire region.

The objective of wave-domain adaptive ANC is to design the loudspeaker driving signals $\boldsymbol{d}(k)$ based on the wave-domain residual signal $\alpha_m(k)$ and the acoustic transfer function $\boldsymbol{T}(k)$, so that the noise field $\boldsymbol{v}(\boldsymbol{x},k)$ is canceled by the generated secondary sound field $\boldsymbol{S}(\boldsymbol{x},k)$ over the control region of interest. The proposed ANC algorithms are introduced in the following section.

III. Multi-channel Wave-domain Active Noise Control

We adopt a block-wise operation and transform the microphone measurements into time-frequency domain, and decompose the noise field into the wave-domain coefficients using (9).

In the wave-domain adaptive algorithm, the residual signals in each iteration (the n^{th} time block) can be expressed as

$$\boldsymbol{\alpha}(n,k) = \boldsymbol{\beta}(n,k) + \boldsymbol{\gamma}(n,k), \tag{10}$$

where $\boldsymbol{\alpha}(n,k) = [\alpha_{-M}(n,k), \ldots, \alpha_M(n,k)]^T$, the superscript $(\cdot)^T$ denotes the transpose of a vector, $\boldsymbol{\beta}(n) = [\beta_{-M}(n,k), \ldots, \beta_M(n,k)]^T$ and $\boldsymbol{\gamma}(n,k) = [\gamma_{-M}(n,k), \ldots, \gamma_M(n,k)]^T$.
Here onwards, we omit the dependency k in each vector for notational simplicity, thus have

$$\boldsymbol{\alpha}(n) = \boldsymbol{\beta}(n) + \boldsymbol{\gamma}(n). \tag{11}$$

Below we derive different wave-domain adaptive algorithms by solving two minimization problems, (a) squared residual signal coefficients, and (b) acoustic potential energy.

A. Minimization of squared residual signal coefficients

Minimizing the sum of the squared residual signal coefficients, the cost function becomes

$$\xi_1(n) = \sum_{m=-M}^{M} |\alpha_m(n)|^2 = \boldsymbol{\alpha}^H(n)\boldsymbol{\alpha}(n), \tag{12}$$

where the superscript $(\cdot)^H$ denotes the conjugate transpose. Using the steepest descent algorithm, the adaptive algorithm follows the update equation

$$\boldsymbol{w}(n+1) = \boldsymbol{w}(n) - \frac{\mu}{2}\boldsymbol{\nabla}\xi_1(n), \tag{13}$$

where $\boldsymbol{w}$ is the update variable, μ is the step size. Below we derive the wave-domain update function for two cases, (1) loudspeaker weights are updated directly, and (2) secondary sound field coefficients are updated directly.

Case 1: Update the loudspeaker weights directly.

If we perform the adaptive process on the loudspeaker weights directly, we can obtain the loudspeaker weights for each iteration from the update equation. In this case, the update variable in (13) can be replaced by $\boldsymbol{d}$, that is $\boldsymbol{w} = \boldsymbol{d} = [d_1, \ldots, d_Q]^T$.

By the complex LMS algorithm [33], taking a derivative of $\xi_1(n)$ with respect to $\boldsymbol{d}$, the gradient of the cost function (Theorem 1) can be written by

$$\nabla\xi_1(n) = 2\boldsymbol{T}^H\boldsymbol{\alpha}(n). \tag{14}$$

The proof is given in Appendix A.
Substituting (14) into (13), the final adaptive equation in wave domain can be written as

$$\boldsymbol{d}(n+1) = \boldsymbol{d}(n) - \mu\boldsymbol{T}^H\boldsymbol{\alpha}(n). \tag{15}$$

The block diagram of the algorithm is shown in Fig. 2.

By replacing the LMS filter by the normalized LMS filter, the final update equation of the normalized wave-domain

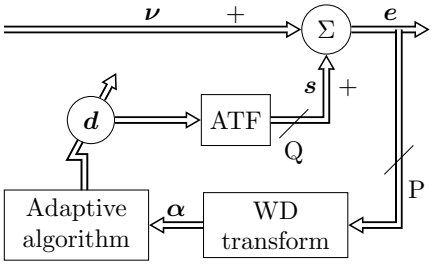

Fig. 2: The block diagram of wave-domain ANC system, when updating the loudspeaker driving signals. Block of WD transform represents the wave-domain transform for the residual signals.

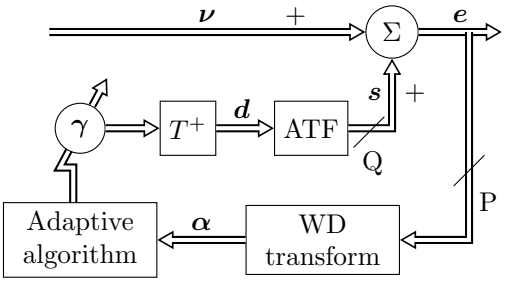

Fig. 3: The block diagram of wave-domain ANC system, when updating the wave-domain coefficients. Block of WD transform represents wave domain transform for the residual signals.

algorithm updating driving signals (NWD-D) can be written as

$$\boldsymbol{d}(n+1) = \boldsymbol{d}(n) - \frac{\mu_0}{\|\boldsymbol{T}^H\|_2^2}\boldsymbol{T}^H\boldsymbol{\alpha}(n), \tag{16}$$

where $\|\cdot\|_2$ denotes the Euclidean norm for a vector or matrix, and $\mu_0 \in [0,1]$ denotes the normalized step size.

Case 2: Update the secondary sound field coefficients.

If we update the wave-domain secondary sound field coefficients ($\boldsymbol{\gamma}$) first, and calculate the loudspeaker driving signals ($\boldsymbol{d}$) later, the update variable in (13) can be replaced by $\boldsymbol{\gamma}$, then we have $\boldsymbol{w} = \boldsymbol{\gamma} = [\gamma_{-M}, \ldots, \gamma_M]^T$. Taking a derivative of $\xi_1(n)$ with respect to $\boldsymbol{\gamma}$, the gradient of the cost function (Theorem 2) can be written by

$$\nabla\xi_1(n) = 2\boldsymbol{\alpha}(n). \tag{17}$$

The proof is given in Appendix B.

Substituting (17) into (13), the adaptive equation in wave-domain coefficients can be written as

$$\boldsymbol{\gamma}(n+1) = \boldsymbol{\gamma}(n) - \mu\boldsymbol{\alpha}(n). \tag{18}$$

Thus, the final update equation of the normalized wave-domain algorithm updating mode coefficients (NWD-M) is as follows,

$$\boldsymbol{\gamma}(n+1) = \boldsymbol{\gamma}(n) - \mu_0\boldsymbol{\alpha}(n). \tag{19}$$

From (8), we obtain the loudspeaker weights $\boldsymbol{d}(n)$ by $\boldsymbol{d} = \boldsymbol{T}^+\boldsymbol{\gamma}$, where the superscript $(\cdot)^+$ denotes the pseudoinverse of a matrix. The block diagram for updating the wave-domain coefficients is shown in Fig 3.

B. The minimization of acoustic potential energy

Minimizing the total acoustic potential energy (APE) in an enclosed noise field can achieve global reduction in sound pressure throughout the enclosure [34], [35]. Here we derive the acoustic potential energy in terms of the wave-domain coefficients to obtain global reduction over the control region.

By definition, acoustic potential energy is

$$E_p(k) = \frac{1}{2\rho_0 c^2}P(k), \tag{20}$$

where ρ_0 denotes the density of the media and $P(k)$ is the average energy of the residual signal given by

$$\begin{aligned} P(k) &= \int_S e^*(\boldsymbol{x},k)e(\boldsymbol{x},k)dS \\ &= \int_0^{2\pi}\int_0^{R_1} e^*(\boldsymbol{x},k)e(\boldsymbol{x},k)rdrd\phi_{\boldsymbol{x}}, \end{aligned} \tag{21}$$

with superscript $(\cdot)^*$ denoting the complex conjugate. Since the potential energy is a scalar multiple of the average spatial energy, by defining $P(k)$ to be the cost function, we can effectively minimize the potential energy.

We represent $P(k)$ in the spherical harmonics domain by substituting (9) into (21) as,

$$P(k) = \sum_{m=-M}^{M}\alpha_m^*(k)\alpha_m(k)\underbrace{(2\pi\int_0^{R_1}(J_m(kr))^2rdr)}_{u_m(k)}, \tag{22}$$

where the integral in (22) is estimated by numerically evaluating the integral between 0 and R_1, which is the integral over the interested region.

Then, (22) can be written in matrix form as

$$P(k) = \boldsymbol{\alpha}^H\boldsymbol{U}\boldsymbol{\alpha}, \tag{23}$$

where $\boldsymbol{\alpha} = [\alpha_{-M}, \ldots, \alpha_M]^T$, $\boldsymbol{U} = \text{diag}(u_{-M}, \ldots, u_{-M})$, and $u_m = 2\pi\int_0^{R_1}(J_m(kr))^2rdr$.

Therefore, the new cost function becomes

$$\xi_p(n) = P(n) = \boldsymbol{\alpha}^H(n)\boldsymbol{U}\boldsymbol{\alpha}(n). \tag{24}$$

where the frequency dependency k is omitted for notational simplicity.

We derive the update equation for the new cost function in two cases.

Case 1: Update the loudspeaker weights directly.

The gradient of the cost function (Theorem 3) can be written by

$$\nabla\xi_p(n) = 2\boldsymbol{T}^H\boldsymbol{U}\boldsymbol{\alpha}(n). \tag{25}$$

The proof is given in Appendix C.

Substituting (25) into (13), the final adaptive equation in wave domain can be written as

$$\boldsymbol{d}(n+1) = \boldsymbol{d}(n) - \mu\boldsymbol{T}^H\boldsymbol{U}\boldsymbol{\alpha}(n). \tag{26}$$

Similar to (16), the update equation of the normalized energy-based wave domain algorithm updating driving signals (NEWD-D) can be written as

$$\boldsymbol{d}(n+1) = \boldsymbol{d}(n) - \frac{\mu_0}{\|\boldsymbol{T}^H\boldsymbol{U}\|_2^2}\boldsymbol{T}^H\boldsymbol{U}\boldsymbol{\alpha}(n). \tag{27}$$

Case 2: Update the secondary sound field coefficients.

The gradient of the cost function (Theorem 4) can be written as

$$\nabla\xi_p(n) = 2\boldsymbol{U}\boldsymbol{\alpha}(n). \tag{28}$$

The proof is given in Appendix D.
Substituting (28) into (13), the adaptive equation in the wave-domain coefficients can be written as

$$\boldsymbol{\gamma}(n+1) = \boldsymbol{\gamma}(n) - \mu\boldsymbol{U}\boldsymbol{\alpha}(n). \tag{29}$$

The final update equation of the normalized energy-based wave domain algorithm updating the mode coefficients (NEWD-M) can be written as

$$\boldsymbol{\gamma}(n+1) = \boldsymbol{\gamma}(n) - \frac{\mu_0}{\|\boldsymbol{U}\|_2^2}\boldsymbol{U}\boldsymbol{\alpha}(n). \tag{30}$$

Then the loudspeaker weights $\boldsymbol{d}(n)$ can be calculated by $\boldsymbol{d} = \boldsymbol{T}^{+}\boldsymbol{\gamma}$ in each iteration.

IV. Simulation results

A. Simulation setup

In this section, performance of the proposed four wave domain algorithms (i) normalized wave domain algorithm updating driving signals (NWD-D), (ii) normalized wave domain algorithm updating mode coefficients (NWD-M), (iii) normalized energy-based wave domain algorithm updating driving signals (NEWD-D), and (iv) normalized energy-based wave domain algorithm updating the mode coefficients (NEWD-M) are compared with the conventional normalized multi-point (NMP) algorithm[2], in both free-field and reverberant environments. We assume the desired control zone to be a circular region of a radius of 1 m (black area in Fig. 1), and the noise field to be generated by point sources, which are outside of the control region.

We utilize a feedback ANC system for control on a 2D plane, where the circular microphone array of radius 1 m is placed on the boundary of the control region and the circular loudspeaker array of radius 2 m is placed outside the control region. The speed of sound is $c = 343$ m/s and the density of the air is $\rho_0 = 1.225$ kg/m^3. The simulation of the reverberant environment is modeled as a rectangular room of size 6 m$\times$6 m with perfectly absorbing ceiling and floor, and all the side walls have a reflection coefficient of 0.75. The reverberation is simulated using the image-source method [36].

The simulation starts in the time domain. We adopt a block-wise operation and transform the microphone recordings into the time-frequency domain. Based on (9), we further transfer the signal into wave-domain coefficients. A sampling rate of 8 kHz and a window length of 3200 samples are employed. White Gaussian noise with signal-to-noise (SNR) ratio of 40 dB is added to each microphone recordings to model the internal thermal noise of microphones.

To evaluate the primary noise reduction performance, we study the (i) instantaneous noise reduction on the microphones $N_{\mathrm{r}}^{\mathrm{b}}(n)$, (ii) noise reduction inside the interest region $N_{\mathrm{r}}^{\mathrm{in}}(n)$, and (iii) acoustic potential energy over region $E_p(n)$.

The instantaneous noise reduction on the microphones can be defined as

$$N_{\mathrm{r}}^{\mathrm{b}}(n) \triangleq 10\log_{10}\frac{\sum_z E\{|e_z(n)|^2\}}{\sum_z E\{|e_z(0)|^2\}}, \tag{31}$$

where $e_z(n)$ represents the sound pressure received on the z^{th} microphones at the n^{th} iteration, and $e_z(0)$ represents the sound pressure received on the z^{th} microphones before the ANC process.

To evaluate the noise reduction performance inside the control region, sound pressure at $L = 1296$ points uniformly placed inside the regions $\boldsymbol{e}_{in}$ are examined. We define the instantaneous noise reduction inside the interest region $N_{\mathrm{r}}^{\mathrm{in}}(n)$ as follows,

$$N_{\mathrm{r}}^{\mathrm{in}}(n) \triangleq 10\log_{10}\frac{\sum_l E\{|e_{\mathrm{in}\_l}(n)|^2\}}{\sum_l E\{|e_{\mathrm{in}\_l}(0)|^2\}}, \tag{32}$$

where $e_{\mathrm{in}\_l}(n)$ denotes the residual signals at the l^{th} point inside the region at the n^{th} iteration, and $e_{\mathrm{in}\_l}(0)$ represents the primary noise field at the l^{th} point in the region.

As mentioned above, acoustic potential energy is another measure of evaluating the noise reduction over the entire spatial region [37], which can be considered as a more insightful measure in practice. From (20) and (23), the acoustic potential energy over the control region for each iteration can be calculated by

$$E_p(n) = \frac{1}{2\rho_0 c^2}\boldsymbol{\alpha}^H(n)\boldsymbol{U}\boldsymbol{\alpha}(n), \tag{33}$$

where $\boldsymbol{\alpha}(n)$ can be conveniently captured by circular microphone arrays, and calculated based on (9).

In addition to the noise reduction measures mentioned above, we analyze two more performance measures, (i) the residual noise field in the control region, and (ii) the convergence speed. We simulate the ANC algorithms to deal with a single frequency noise field and a multi-frequency noise field as shown in the following two subsections.

B. Single frequency

First, we investigate the narrowband performance of different algorithms. Three noise sources are located at $(2.2, 0^\circ)$, $(2.5, 45^\circ)$, and $(3, 240^\circ)$ with magnitude of 10, 15 and 5, which are marked as pink $'+'$ in Fig. 4 and Fig. 5. The frequency of the noise field is 200 Hz. The control region (R_1 = 1 m) in such a noise field can be represented by $m\epsilon[-5, 5]$ modes, thus, we place $2N + 1 = 11$ microphones on the boundary to capture the information of the residual noise field for each modes. We select the same normalized step values for different algorithms, $\mu_0 = 0.8$ in free-field and $\mu_0 = 0.5$ in reverberant environments.

[2]Here, NMP algorithm is the normalized version of the MC algorithm in [10].

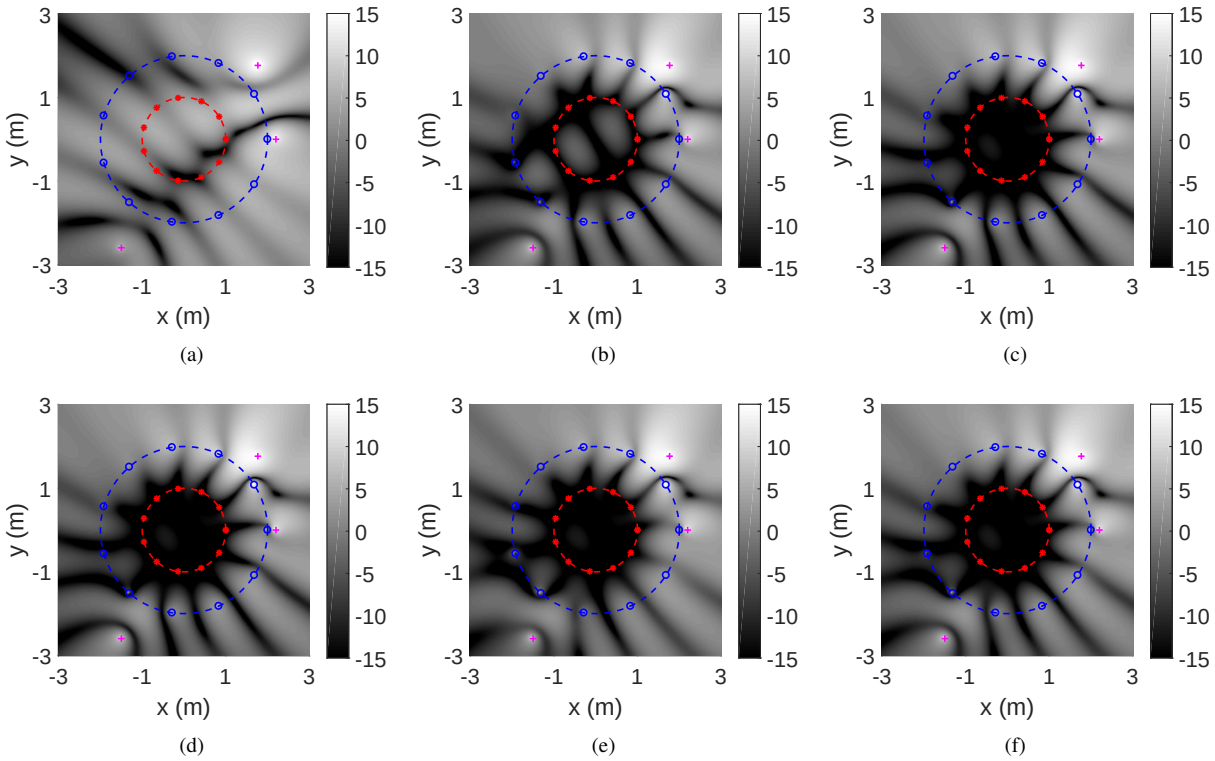

Fig. 4: Noise cancellation performance after 50 iterations using different ANC algorithm in free-field: (a) Primary noise field (200 Hz) (b) Normalized MP (c) NWD-M (d) NWD-D (e) NEWD-M (f) NEWD-D.

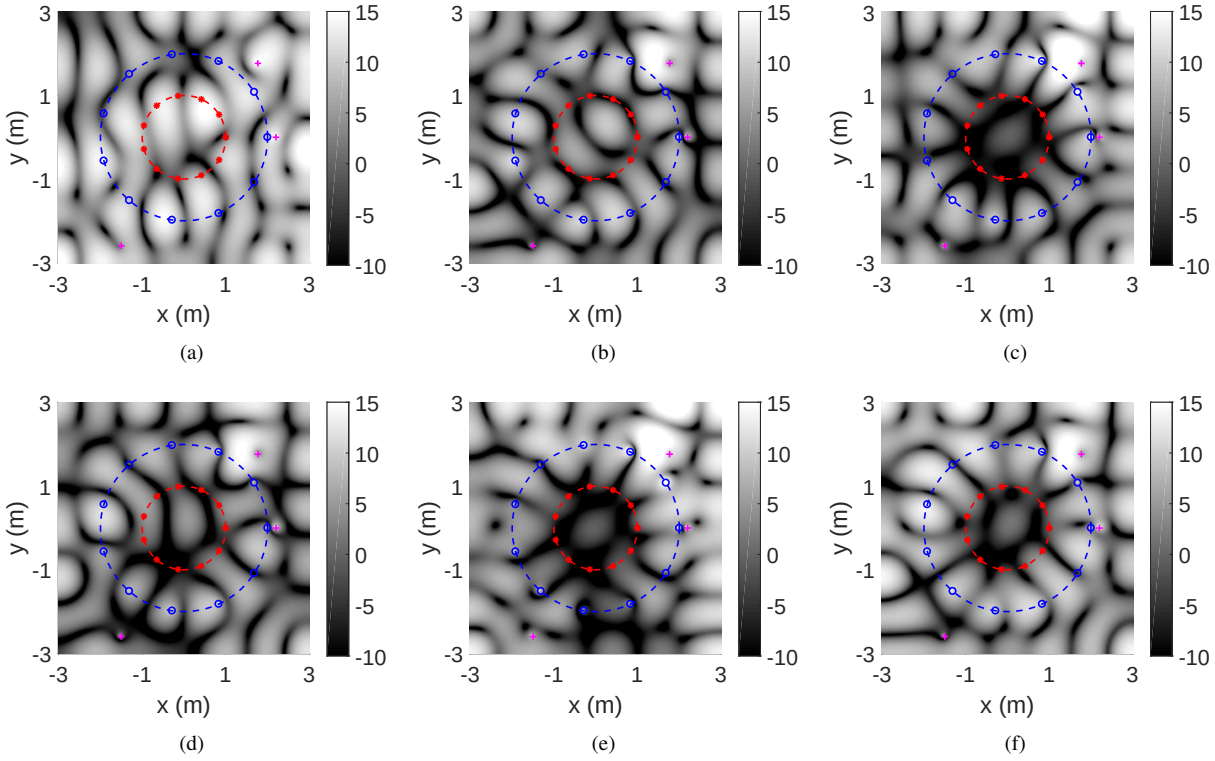

Fig. 5: Noise cancellation performance after 50 iterations using different ANC algorithm in reverberant environments: (a) primary noise field (200 Hz) (b)Normalized MP (c) NWD-M (d) NWD-D (e) NEWD-M (f) NEWD-D.

1) Loudspeaker number meeting the requirement: In order to control all the modes in the entire spatial region, $2N+1 = 11$ loudspeakers are required to be placed in the corresponding array.

Fig. 4 and Fig. 5 demonstrate the energy of residual noise fields over region before ANC and after 50 iterations of ANC process, in free-field and in reverberant environments. NWD-D, NWD-M, NEWD-D and NEWD-M can achieve noise cancellation over the entire region. Whereas NMP can only reduce the noise on the boundary close to the microphone points after 50 iterations. Compared to the primary noise field (Fig. 4(a) and Fig. 5(a)), we can see that all the wave domain methods can achieve higher noise reduction over the entire region than the NMP method, in both free-field and reverberation environments within 50 iterations.

Fig. 6, Fig. 7, Fig. 8 and Fig. 9 compare the noise reduction level and convergence performance for each algorithm in free-field and in a room environment. Fig. 6 and Fig. 8 are zoomed in versions of Fig. 7 and Fig. 9 in the first 50 iterations, respectively. The acoustic potential energy reduction over region shows a similar trend to the noise reduction over region, as they both monitor the overall energy of the control region.

From Fig. 7 and Fig. 9, we can see that all the wave domain algorithms can cancel the noise on the boundary and over the entire region. In the steady state, different algorithms can achieve similar $N_{\mathrm{r}}^{\mathrm{in}}(n)$ attenuation, the same for $N_{\mathrm{r}}^{\mathrm{b}}(n)$ and APE reduction.

Fig. 6 and Fig. 8 demonstrate the convergence speed in free field and in room reverberant environment. NMP converges fast on the boundary, but much slower inside the region. In free field, coefficients-based algorithms (NWD-M and NWD-D) converge faster than the energy-based WD algorithms. In room reverberant environment, algorithms updating wave coefficients (NWD-M and NEWD-M) have better convergence performance than the algorithms updating driving signals directly (NWD-D and NEWD-D). For the comparison of the free-field case and room case, we can see that NWD-M has the fastest convergence speed both in free-field and in reverberant environment. While NWD-D works well in the free-field, but converges much slower in a room.

2) Loudspeaker number less than the requirement: In real applications, it is possible that the secondary sources are limited, so that less numbers of loudspeaker are available than the requirement $(2N + 1)$. In the simulation below, a small number of loudspeakers are equi-angularly placed in the circular array, which can not cover all the modes in the spatial region.

Fig. 10 demonstrates the convergence performance in the reverberant environment using 9 loudspeakers. The algorithms updating mode coefficients converge faster than the algorithms updating driving signals directly. The NMP algorithm has the slowest convergence rate. Since 9 loudspeakers can not reconstruct all the modes in the control region, the noise reduction performance in the steady state degrades significantly compared to that of using 11 loudspeakers. By minimizing the weighted $(u_m(k))$ squared sum of the wave domain residual signals, the energy-based wave domain algorithms emphasize the importance of the low order modes, and reduce the

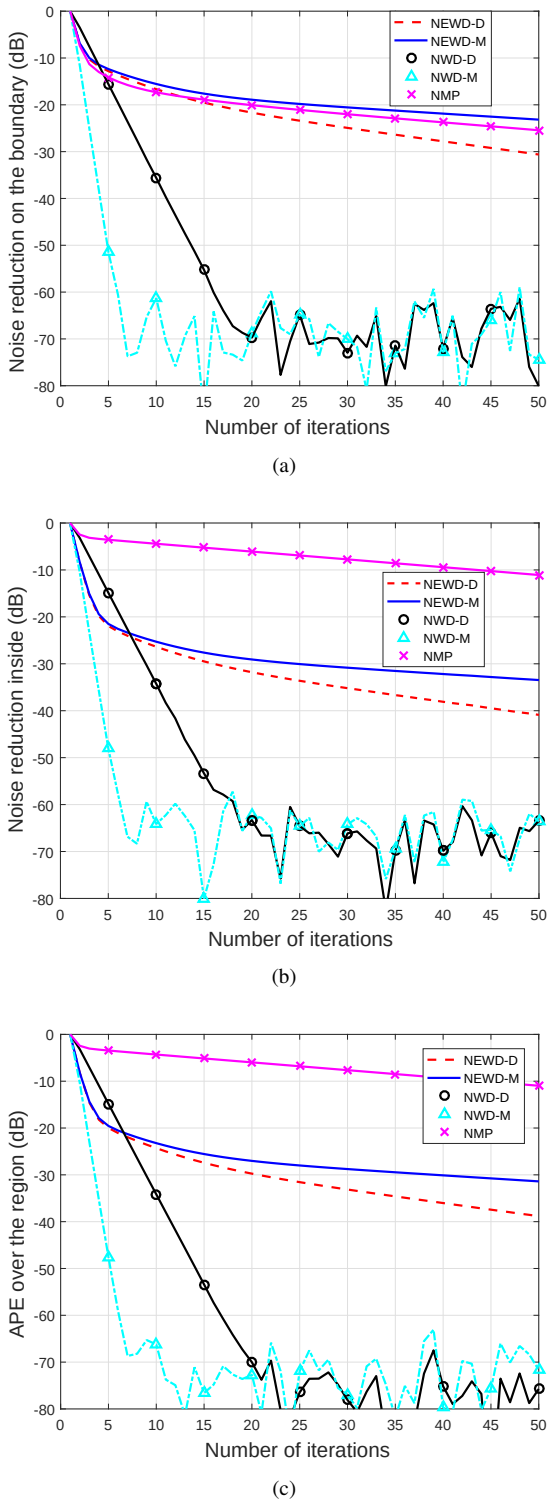

Fig. 6: Convergence performance using different ANC algorithm in free-field (50 iterations): (a) noise reduction on the boundary (b) noise reduction inside the region (c) acoustic potential energy reduction over the region.

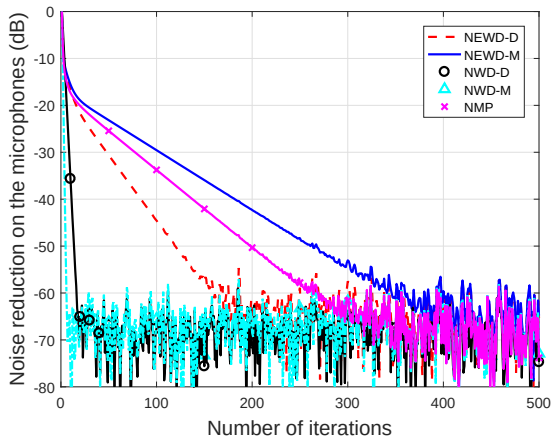

(a)

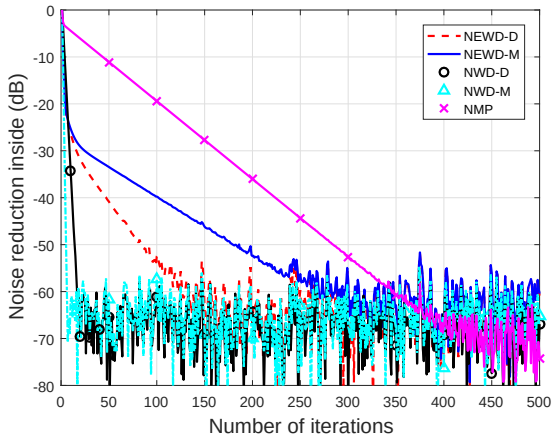

(b)

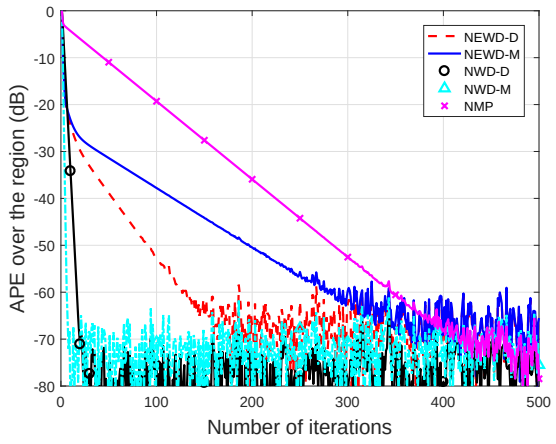

(c)

Fig. 7: Convergence performance using different ANC algorithm in free-field (500 iterations): (a) noise reduction on the boundary (b) noise reduction inside the region (c) acoustic potential energy reduction over the region.

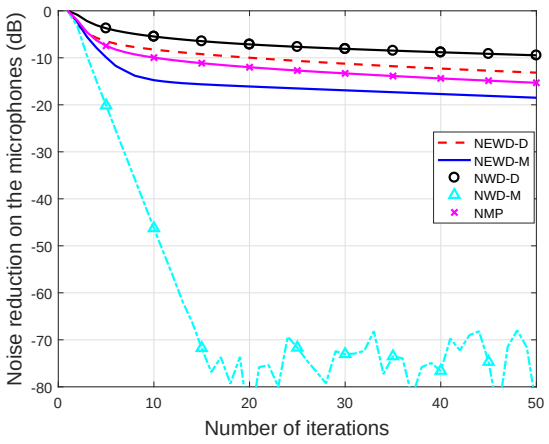

(a)

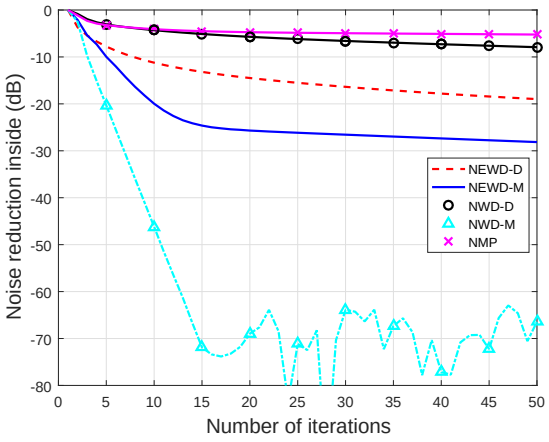

(b)

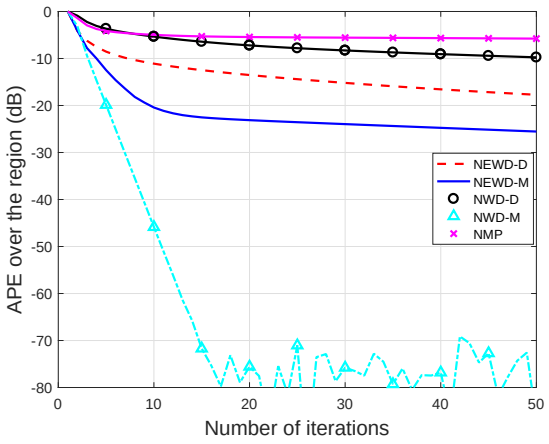

(c)

Fig. 8: Convergence performance using different ANC algorithm in reverberant environment (50 iterations): (a) noise reduction on the boundary (b) noise reduction inside the region (c) acoustic potential energy reduction over the region.

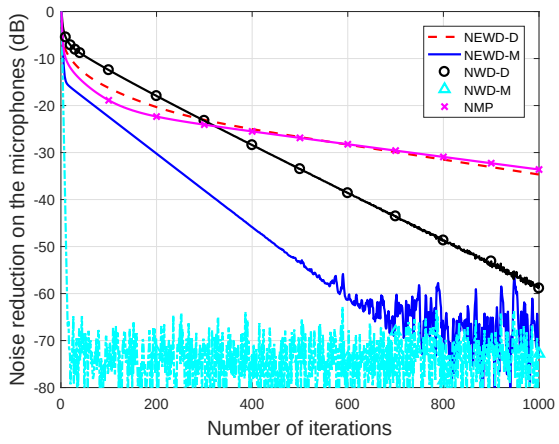

(a)

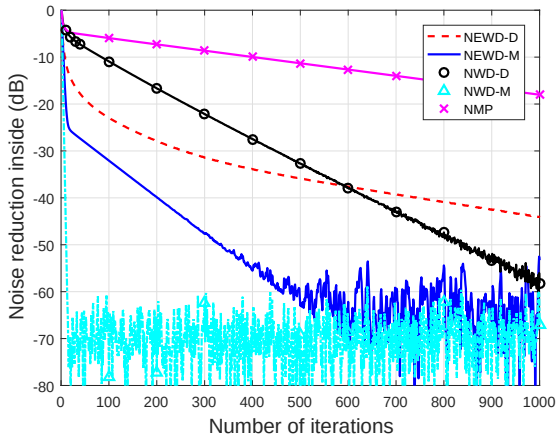

(b)

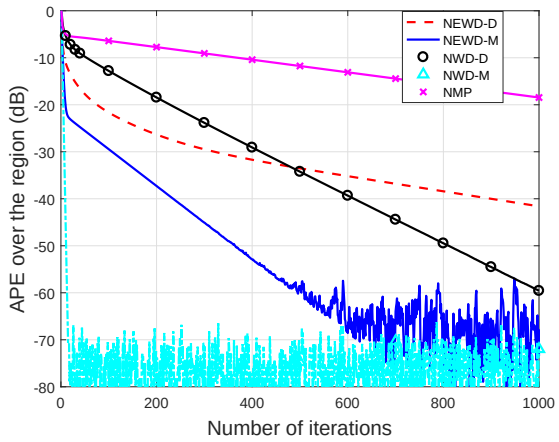

(c)

Fig. 9: Convergence performance using different ANC algorithm in reverberant environment (1000 iterations): (a) noise reduction on the boundary (b) noise reduction inside the region (c) acoustic potential energy reduction over the region.

importance of the high order modes. Therefore, it is found that the energy-based wave domain algorithms (NEWD-D and NEWD-M) can achieve more noise reduction over the entire control region than the other algorithms. Meanwhile, in the steady state the wave domain algorithms have better NR_{in} and APE attenuation performance compared to NMP algorithm.

We further reduce the loudspeaker number to 7 and 5, and evaluate the noise cancellation performance after 1000 iterations, as shown in Table I. NEWD-D and NEWD-M outperform the other algorithms in each case. In general, a smaller loudspeaker number decreases the noise reduction performance, especially the NR_{in} and APE attenuation. For example, when 5 loudspeakers are used, all the algorithms cannot achieve more than -10 dB noise reduction, which indicates deteriorated ANC performance.

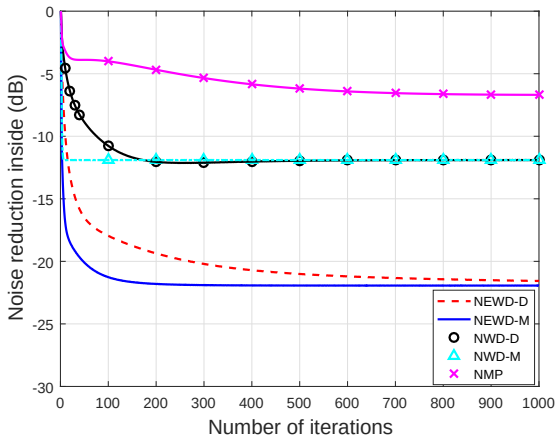

(a)

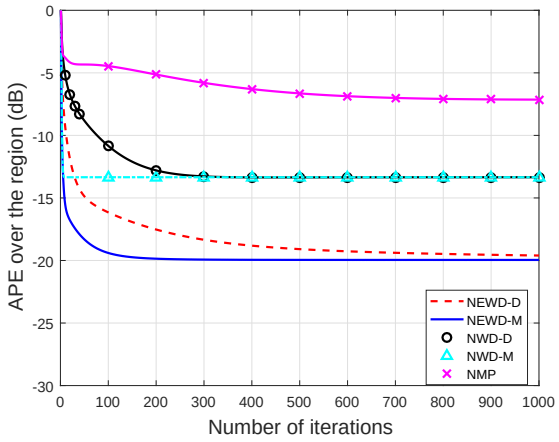

(b)

Fig. 10: Convergence performance using 9 loudspeakers in reverberant environment (1000 iterations): (a) noise reduction inside the region (b) acoustic potential energy reduction over the region.

3) Loudspeaker energy consumption: To evaluate the loudspeaker energy consumption during the ANC process, we

TABLE I: Attenuation level using different numbers of loudspeakers.

	N_r^{in} (dB)			APE (dB)		
	9	7	5	9	7	5
NEWD-D	-22	-14	-4	-20	-14	-5
NEWD-M	-22	-14	-4	-20	-14	-5
NWD-D	-12	-6	-1	-13	-7	-2
NWD-M	-12	-6	-1	-13	-7	-2
NMP	-7	-5	0	-7	-5	-1

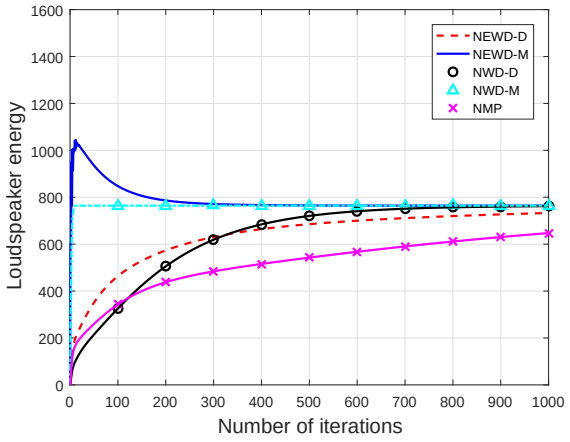

(a)

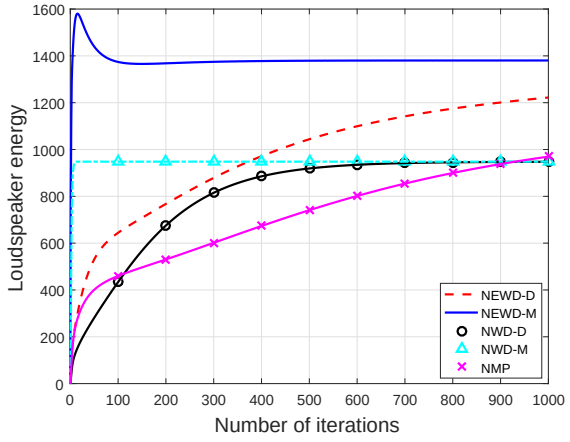

(b)

Fig. 11: Loudspeaker energy ($\boldsymbol{d}^T\boldsymbol{d}$) using different ANC algorithms during 1000 iterations in reverberant environment: (a) 11 loudspeakers (b) 9 loudspeakers.

compare the total energy of all the loudspeakers[3] ($\boldsymbol{d}^T\boldsymbol{d}$) using different algorithms in the reverberant environment, as shown in Fig. 11.

When 11 loudspeakers are utilized to generate the secondary sound field (Fig. 11(a)), the algorithms which update the driving signals will gradually increase the total energy, and reach the steady state smoothly. While the loudspeaker energy using NEWD-M will have a peak before the steady state. All the algorithms will reach the same energy level after convergence. When we have limited resources, the loudspeakers consume more energy to achieve the noise cancellation, as shown in Fig. 11(b). Meanwhile, the energy-based algorithms will end up with more loudspeaker energy, compared to the other algorithms.

[3]Here, we evaluate the summation of squared driving signals, for all the 11 loudspeakers.

C. Multi-frequency

For broadband noise field, we assume that only one noise source is located at $(2.5, 0°)$, and it can be synthesised by the combination of $J = 19$ dominant narrowband components. The frequency range is from 50 Hz to 500 Hz with the same pressure level in each frequency bin $f_j, j = 1, 2, ..., J$. The system is designed for the frequency upper bound, so that we place $2M + 1 = 27$ loudspeakers and 27 microphones in each corresponding array.

The noise reduction performance inside the control region in free field and reverberant environments are shown in Fig. 12 and Fig. 13 respectively. Over a wide frequency range, the wave-domain ANC algorithms can cancel the noise inside the entire region. In free-field, the average noise reduction is around -25 dB and -50 dB, for energy-based WD algorithms and WD algorithms, respectively. Similarly results have been shown in reverberant environments. Notice that the noise reduction performance is significantly degraded at 300 Hz and 475 Hz. This is due to the 'irregular frequencies' problem, where the Bessel functions in the corresponding frequencies are closed to zero and the coefficient errors are amplified. This is a limitation of the wave domain technique when using a single circular microphone array. However, there are well understood methods to tackle this problem such as using two closely spaced microphone arrays [32], [38], using multi-radii shell array [39], and using a planar array of differential microphones [40]. In the reverberant environments, the variation of N_r^{in} and APE reduction between different frequency bin are relatively larger than in the free-field, especially for the WD algorithms.

V. Conclusion

In this paper, wave-domain adaptive algorithms are developed for active noise control over spatial regions resulting in four algorithms. Simulation results show that all four variants of the wave domain algorithms can achieve significant noise reduction over the entire spatial regions, and perform faster convergence compared with the conventional multi-point method in both free-field and reverberant environments. When the number of loudspeakers is large enough to cover all active modes in the control region, all algorithms, including conventional multi-point method, can reach the same noise reduction level in steady state. However, algorithms updating wave-domain coefficients have the fastest convergence performance. When the number of loudspeakers is limited and less than the number of active modes of the region, the energy-based wave domain algorithms will have better performance than the other algorithms, in terms of noise attenuation and the convergence speed. Analysing the stability of different algorithms and extending these wave-domain ANC approaches to the 3-D noise

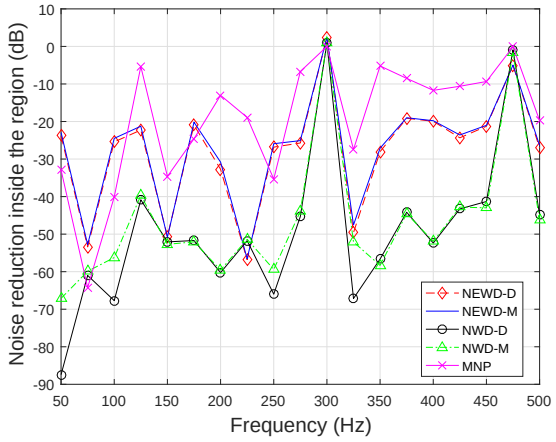

(a)

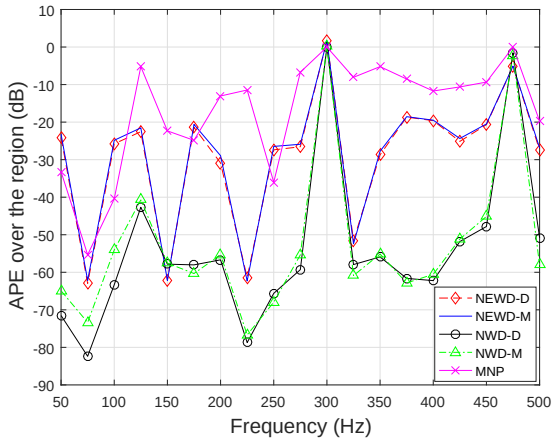

(b)

Fig. 12: Multi-frequency performance using different wave-domain ANC algorithm in free-field after 50 iterations: (a) noise reduction inside the region (b) acoustic potential energy reduction over the region.

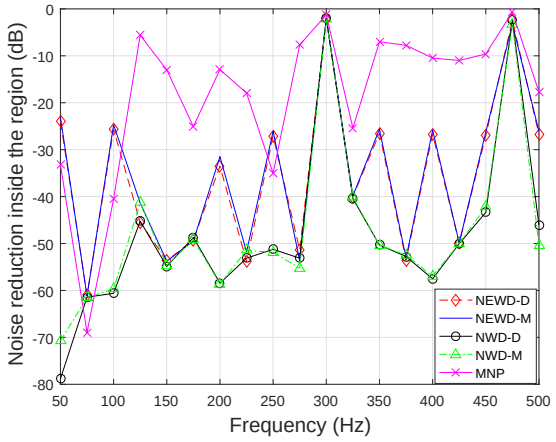

(a)

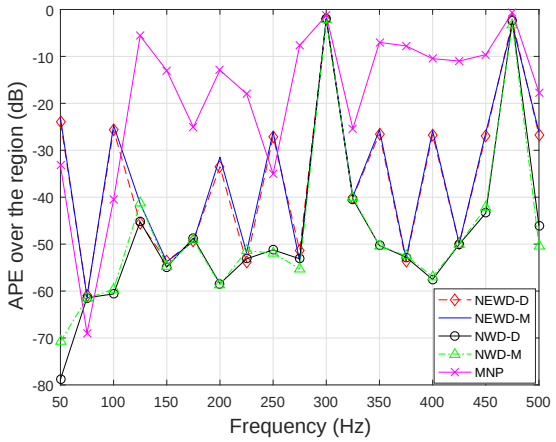

(b)

Fig. 13: Multi-frequency performance using different wave-domain ANC algorithm in reverberant environment after 50 iterations: (a) noise reduction inside the region (b) acoustic potential energy reduction over the region.

cancellation using spherical harmonics analysis are topics for the future work.

APPENDIX A
PROOF OF THEOREM 1

The gradient vector and the conjugate derivative [41] are related by

$$\nabla\xi_1 = 2\frac{\partial\xi_1}{\partial \boldsymbol{d}^*} = 2\frac{\partial(\boldsymbol{\alpha}^H\boldsymbol{\alpha})}{\partial \boldsymbol{d}^*}, \tag{34}$$

where we use (12) and omit the iteration index n for notational simplicity.
Substitute (8) and (11) into (34),

$$\nabla\xi_1 = 2\bigg(\frac{\partial(\boldsymbol{\beta}^H\boldsymbol{\beta})}{\partial \boldsymbol{d}^*} + \frac{\partial(\boldsymbol{\beta}^H\boldsymbol{T}\boldsymbol{d})}{\partial \boldsymbol{d}^*} + \frac{\partial(\boldsymbol{d}^H\boldsymbol{T}^H\boldsymbol{\beta})}{\partial \boldsymbol{d}^*} + \frac{\partial(\boldsymbol{d}^H\boldsymbol{T}^H\boldsymbol{T}\boldsymbol{d})}{\partial \boldsymbol{d}^*}\bigg). \tag{35}$$

Calculate each items separately to get,

$$\begin{aligned}\frac{\partial(\boldsymbol{\beta}^H\boldsymbol{\beta})}{\partial \boldsymbol{d}^*} &= \frac{\partial(\boldsymbol{\beta}^H\boldsymbol{T}\boldsymbol{d})}{\partial \boldsymbol{d}^*} = 0,\\ \frac{\partial(\boldsymbol{d}^H\boldsymbol{T}^H\boldsymbol{\beta})}{\partial \boldsymbol{d}^*} &= \boldsymbol{T}^H\boldsymbol{\beta},\\ \frac{\partial(\boldsymbol{d}^H\boldsymbol{T}^H\boldsymbol{T}\boldsymbol{d})}{\partial \boldsymbol{d}^*} &= \boldsymbol{T}^H\boldsymbol{T}\boldsymbol{d}.\end{aligned} \tag{36}$$

Substituting (36) into (35),

$$\nabla\xi_1 = 2\boldsymbol{T}^H(\boldsymbol{\beta} + \boldsymbol{T}\boldsymbol{d}). \tag{37}$$

Substituting (8) and (11) into (37), we complete the proof.

APPENDIX B
PROOF OF THEOREM 2

The gradient vector and the conjugate derivative are related by

$$\nabla\xi_1 = 2\frac{\partial\xi}{\partial\boldsymbol{\gamma}^*} = 2\frac{\partial(\boldsymbol{\alpha}^H\boldsymbol{\alpha})}{\partial\boldsymbol{\gamma}^*}. \tag{38}$$

Substitute (8) and (11) into (38),

$$\nabla\xi_1 = 2\left(\frac{\partial(\boldsymbol{\beta}^H\boldsymbol{\beta})}{\partial\boldsymbol{\gamma}^*} + \frac{\partial(\boldsymbol{\beta}^H\boldsymbol{\gamma})}{\partial\boldsymbol{\gamma}^*} + \frac{\partial(\boldsymbol{\gamma}^H\boldsymbol{\beta})}{\partial\boldsymbol{\gamma}^*} + \frac{\partial(\boldsymbol{\gamma}^H\boldsymbol{\gamma})}{\partial\boldsymbol{\gamma}^*}\right). \tag{39}$$

Calculate each items separately,

$$\frac{\partial(\boldsymbol{\beta}^H\boldsymbol{\beta})}{\partial\boldsymbol{\gamma}^*} = \frac{\partial(\boldsymbol{\beta}^H\boldsymbol{\gamma})}{\partial\boldsymbol{\gamma}^*} = 0,$$

$$\frac{\partial(\boldsymbol{\gamma}^H\boldsymbol{\beta})}{\partial\boldsymbol{\gamma}^*} = \boldsymbol{\beta},$$

$$\frac{\partial(\boldsymbol{\gamma}^H\boldsymbol{\gamma})}{\partial\boldsymbol{\gamma}^*} = \boldsymbol{\gamma}. \tag{40}$$

Substituting (11) and (40) into (39), we complete the proof.

APPENDIX C
PROOF OF THEOREM 3

The gradient vector and the conjugate derivative [41] are related by

$$\nabla\xi_p = 2\frac{\partial\xi_p}{\partial\boldsymbol{d}^*}, \tag{41}$$

where the iteration index n has been omitted for notational simplicity.
Therefore the gradient is expressed as

$$\nabla\xi_p = 2\frac{\partial(\boldsymbol{\alpha}^H\boldsymbol{U}\boldsymbol{\alpha})}{\partial\boldsymbol{d}^*}. \tag{42}$$

Substitute (8) and (11) into (42),

$$\nabla\xi_p = 2\Bigg(\frac{\partial(\boldsymbol{\beta}^H\boldsymbol{U}\boldsymbol{\beta})}{\partial\boldsymbol{d}^*} + \frac{\partial(\boldsymbol{\beta}^H\boldsymbol{U}\boldsymbol{T}\boldsymbol{d})}{\partial\boldsymbol{d}^*} + \frac{\partial(\boldsymbol{d}^H\boldsymbol{T}^H\boldsymbol{U}\boldsymbol{\beta})}{\partial\boldsymbol{d}^*} + \frac{\partial(\boldsymbol{d}^H\boldsymbol{T}^H\boldsymbol{U}\boldsymbol{T}\boldsymbol{d})}{\partial\boldsymbol{d}^*}\Bigg). \tag{43}$$

Calculate each items separately,

$$\frac{\partial(\boldsymbol{\beta}^H\boldsymbol{U}\boldsymbol{\beta})}{\partial\boldsymbol{d}^*} = \frac{\partial(\boldsymbol{\beta}^H\boldsymbol{U}\boldsymbol{T}\boldsymbol{d})}{\partial\boldsymbol{d}^*} = 0,$$

$$\frac{\partial(\boldsymbol{d}^H\boldsymbol{T}^H\boldsymbol{U}\boldsymbol{\beta})}{\partial\boldsymbol{d}^*} = \boldsymbol{T}^H\boldsymbol{U}\boldsymbol{\beta},$$

$$\frac{\partial(\boldsymbol{d}^H\boldsymbol{T}^H\boldsymbol{U}\boldsymbol{T}\boldsymbol{d})}{\partial\boldsymbol{d}^*} = \boldsymbol{T}^H\boldsymbol{U}\boldsymbol{T}\boldsymbol{d}. \tag{44}$$

Substituting (44) into (43),

$$\nabla\xi_p = 2\boldsymbol{T}^H\boldsymbol{U}(\boldsymbol{\beta} + \boldsymbol{T}\boldsymbol{d}). \tag{45}$$

Substituting (8) and (11) into (45), we complete the proof.

APPENDIX D
PROOF OF THEOREM 4

The gradient vector and the conjugate derivative are related by

$$\nabla\xi_p = 2\frac{\partial\xi_p}{\partial\boldsymbol{\gamma}^*} = 2\frac{\partial(\boldsymbol{\alpha}^H\boldsymbol{U}\boldsymbol{\alpha})}{\partial\boldsymbol{\gamma}^*}. \tag{46}$$

Substitute (8) and (11) into (46),

$$\nabla\xi_p = 2\Bigg(\frac{\partial(\boldsymbol{\beta}^H\boldsymbol{U}\boldsymbol{\beta})}{\partial\boldsymbol{\gamma}^*} + \frac{\partial(\boldsymbol{\beta}^H\boldsymbol{U}\boldsymbol{\gamma})}{\partial\boldsymbol{\gamma}^*} + \frac{\partial(\boldsymbol{\gamma}^H\boldsymbol{U}\boldsymbol{\beta})}{\partial\boldsymbol{\gamma}^*} + \frac{\partial(\boldsymbol{\gamma}^H\boldsymbol{U}\boldsymbol{\gamma})}{\partial\boldsymbol{\gamma}^*}\Bigg). \tag{47}$$

Calculate each items separately,

$$\frac{\partial(\boldsymbol{\beta}^H\boldsymbol{U}\boldsymbol{\beta})}{\partial\boldsymbol{\gamma}^*} = \frac{\partial(\boldsymbol{\beta}^H\boldsymbol{U}\boldsymbol{\gamma})}{\partial\boldsymbol{\gamma}^*} = 0,$$

$$\frac{\partial(\boldsymbol{\gamma}^H\boldsymbol{U}\boldsymbol{\beta})}{\partial\boldsymbol{\gamma}^*} = \boldsymbol{U}\boldsymbol{\beta},$$

$$\frac{\partial(\boldsymbol{\gamma}^H\boldsymbol{U}\boldsymbol{\gamma})}{\partial\boldsymbol{\gamma}^*} = \boldsymbol{U}\boldsymbol{\gamma}. \tag{48}$$

Substituting (11) and (48) into (47), we complete the proof.

REFERENCES

[1] C. C. Fuller, S. Elliott, and P. A. Nelson, *Active Control of Vibration*. San Diego, CA: Academic, 1996.

[2] S. M. Kuo and A. B. Puvvala, "Effects of frequency separation in periodic active noise control systems," *IEEE Trans. Audio, Speech, Language Process.*, vol. 14, no. 5, pp. 1857–1866, Sep. 2006.

[3] S. Elliot, P. Nelson, I. Stothers, and C. Boucher, "In-flight experiments on the active control of propeller-induced cabin noise," *J. Sound Vibration*, vol. 140, no. 2, pp. 219 – 238, 1990.

[4] H. Sano, T. Inoue, A. Takahashi, K. Terai, and Y. Nakamura, "Active control system for low-frequency road noise combined with an audio system," *IEEE Trans. Speech, Audio Process.*, vol. 9, no. 7, pp. 755–763, Oct. 2001.

[5] J. Cheer and S. J. Elliott, "The design and performance of feedback controllers for the attenuation of road noise in vehicles," *International Journal of Acoustics and Vibration*, vol. 19, no. 3, pp. 155–164, Jan. 2014.

[6] ——, "Multichannel control systems for the attenuation of interior road noise in vehicles," *Mech. Syst. Signal Process.*, vol. 6061, pp. 753 – 769, 2015.

[7] P. N. Samarasinghe, W. Zhang, and T. D. Abhayapala, "Recent advances in active noise control inside automobile cabins: Toward quieter cars," *IEEE Signal Process. Mag.*, vol. 33, no. 6, pp. 61–73, Nov. 2016.

[8] A. Kuntz and R. Rabenstein, "An approach to global noise control by wave field synthesis," in *2004 12th European Signal Processing Conference*, Sept 2004, pp. 1999–2002.

[9] Y. Kajikawa, W.-S. Gan, and S. M. Kuo, "Recent advances on active noise control: Open issues and innovative applications," *APSIPA Transactions on Signal and Information Processing*, vol. 1, p. 21, Apr. 2012.

[10] J. Zhang, T. D. Abhayapala, P. N. Samarasinghe, W. Zhang, and S. Jiang, "Multichannel active noise control for spatially sparse noise fields," *J. Acoust. Soc. Am.*, vol. 140, no. 6, pp. EL510–EL516, Dec. 2016.

[11] A. Barkefors, M. Sternad, and L.-J. Brännmark, "Design and analysis of linear quadratic gaussian feedforward controllers for active noise control," *IEEE/ACM Trans. Audio, Speech, Language Process.*, vol. 22, no. 12, pp. 1777–1791, 2014.

[12] S. M. Kuo and D. R. Morgan, "Active noise control: A tutorial review," *Proc. IEEE*, vol. 87, no. 6, pp. 943–973, Jun. 1999.

[13] J. Cheer, "Active control of the acoustic environment in an automobile cabin," Ph.D. dissertation, University of Southampton, 2012.

[14] Q. Shen and A. Spanias, "Frequency-domain adaptive algorithms for multi-channel active sound control," in *Proc. Recent Advances in Active Control of Sound Vibration*, 1993, pp. 755–766.

[15] T. Kosaka, S. Elliott, and C. Boucher, "A novel frequency domain filtered-x LMS algorithm for active noise reduction," in *Proc. IEEE Int. Conf. Acoust., Speech, Signal Process. 1997*, vol. 1, Munich, Germany, Apr. 1997, pp. 403–406.

[16] J. Benesty and D. Morgan, "Frequency-domain adaptive filtering revisited, generalization to the multi-channel case, and application to acoustic echo cancellation," in *Proc. IEEE Int. Conf. Acoust., Speech, Signal Process. 2000*, vol. 2, Istanbul, Turkey, Jun. 2000, pp. II789–II792.

[17] J. Lorente, M. Ferrer, M. De Diego, and A. González, "GPU implementation of multichannel adaptive algorithms for local active noise control," *IEEE/ACM Trans. Audio, Speech, Language Process.*, vol. 22, no. 11, pp. 1624–1635, Nov. 2014.

[18] J. W. Parkins, S. D. Sommerfeldt, and J. Tichy, "Error analysis of a practical energy density sensor," *J. Acoust. Soc. Am.*, vol. 108, no. 1, pp. 211–222, 2000.

[19] ——, "Narrowband and broadband active control in an enclosure using the acoustic energy density," *J. Acoust. Soc. Am.*, vol. 108, no. 1, pp. 192–203, 2000.

[20] J. Romeu, A. Balastegui, T. Pàmies, and R. Arcos, "Optimal acoustic error sensing for global active control in a harmonically excited enclosure," *Acoustical Physics*, vol. 60, no. 1, pp. 77–85, 2014.

[21] B. Xu and S. D. Sommerfeldt, "Generalized acoustic energy density based active noise control in single frequency diffuse sound fields," *J. Acoust. Soc. Am.*, vol. 136, no. 3, pp. 1112–1119, 2014.

[22] A. Montazeri, J. Poshtan, and M. H. Kahaei, "Analysis of the global reduction of broadband noise in a telephone kiosk using a MIMO modal ANC system," *Int. J. Eng. Sci.*, vol. 45, no. 28, pp. 679 – 697, 2007.

[23] P. Peretti, S. Cecchi, L. Palestini, and F. Piazza, "A novel approach to active noise control based on wave domain adaptive filtering," in *2007 IEEE Workshop on Applications of Signal Processing to Audio and Acoustics*, New Paltz, NY, USA, Oct. 2007, pp. 307–310.

[24] S. Spors and H. Buchner, "An approach to massive multichannel broadband feedforward active noise control using wave-domain adaptive filtering," in *2007 IEEE Workshop on Applications of Signal Processing to Audio and Acoustics*, Oct 2007, pp. 171–174.

[25] ——, "Efficient massive multichannel active noise control using wave-domain adaptive filtering," in *Proc. 3rd International Symposium on Communications, Control and Signal Processing*, St. Julians, Malta, Mar. 2008, pp. 1480–1485.

[26] J. Zhang, W. Zhang, and T. D. Abhayapala, "Noise cancellation over spatial regions using adaptive wave domain processing," in *Proc. IEEE Workshop on Applications of Signal Processing to Audio and Acoustics 2015*, New Paltz, NY, USA, Oct. 2015.

[27] J. Zhang, T. D. Abhayapala, P. N. Samarasinghe, W. Zhang, and S. Jiang, "Sparse complex FxLMS for active noise cancellation over spatial regions," in *Proc. IEEE Int. Conf. Acoust., Speech and Signal Process. 2016*, Shanghai, China, Mar. 2016, pp. 524–528.

[28] J. Cheer and S. J. Elliott, "Active noise control of a diesel generator in a luxury yacht," *Applied Acoustics*, vol. 105, pp. 209 – 214, 2016.

[29] G. Williams, *Fourier Acoustics: Sound Radiation and Nearfield Acoustical Holography*. Academic press, 1999.

[30] R. Kennedy, P. Sadeghi, T. D. Abhayapala, and H. M. Jones, "Intrinsic limits of dimensionality and richness in random multipath fields," *IEEE Trans. Signal Process.*, vol. 55, no. 6, pp. 2542–2556, Jun. 2007.

[31] T. D. Abhayapala, T. Pollock, and R. Kennedy, "Characterization of 3D spatial wireless channels," in *2003 IEEE 58th Vehicular Technology Conference VTC 2003-Fall*, vol. 1, Orlando, FL, USA, Oct. 2003, pp. 123–127.

[32] T. Betlehem and T. D. Abhayapala, "Theory and design of sound field reproduction in reverberant rooms," *J. Acoust. Soc. Am.*, vol. 117, no. 4, pp. 2100–2111, Apr. 2005.

[33] B. Widrow, J. McCool, and M. Ball, "The complex LMS algorithm," *Proc. IEEE*, vol. 63, no. 4, pp. 719–720, Apr. 1975.

[34] M. R. Bai and S. Chang, "Active noise control of enclosed harmonic fields by using BEM-based optimization techniques," *Applied Acoustics*, vol. 48, no. 1, pp. 15–32, 1996.

[35] J. Romeu, A. Balastegui, T. Pamies, and R. Arcos, "Optimal acoustic error sensing for global active control in a harmonically excited enclosure," *Acoustical Physics*, vol. 60, no. 1, pp. 77–85, 2014.

[36] J. B. Allen and D. A. Berkley, "Image method for efficiently simulating small-room acoustics," *J. Acoust. Soc. Am.*, vol. 65, no. 4, pp. 943–950, 1979.

[37] H. Chen, J. Zhang, P. N. Samarasinghe, and T. D. Abhayapala, "Evaluation of spatial active noise cancellation performance using spherical harmonic analysis," in *Proc. IEEE International Workshop on Acoustic Signal Enhancement 2016*, Xi'an, China, Sep. 2016, pp. 1–5.

[38] I. Balmages and B. Rafaely, "Open-sphere designs for spherical microphone arrays," *IEEE Transactions on Audio, Speech, and Language Processing*, vol. 15, no. 2, pp. 727–732, Feb 2007.

[39] B. Rafaely, "The spherical-shell microphone array," *IEEE transactions on audio, speech, and language processing*, vol. 16, no. 4, pp. 740–747, 2008.

[40] H. Chen, T. D. Abhayapala, and W. Zhang, "Theory and design of compact hybrid microphone arrays on two-dimensional planes for three-dimensional soundfield analysis," *The Journal of the Acoustical Society of America*, vol. 138, no. 5, pp. 3081–3092, 2015.

[41] S. Haykin, *Adaptive Filter Theory*. Prentice Hall, 2001.